Materials and Structures (2024) 57:183
https://doi.org/10.1617/s11527-024-02461-4

ORIGINAL ARTICLE

Effects of clay type and component fineness on the hydration and properties of limestone calcined clay cement

Muhammet Atasever · Sinan Turhan Erdoğan

Received: 10 June 2024 / Accepted: 5 September 2024 / Published online: 16 September 2024

Abstract Limestone calcined clay cement (LC^3) is emerging as an alternative to Portland cement, offering economic advantages, reduced CO_2 emissions, and mechanical properties on par with Portland cement. Central to the effective utilization of LC^3 is understanding how the fineness of its components affects its performance. The current study investigates limestone calcined clay cement mixtures composed of kaolinite, illite, and montmorillonite calcined clays and limestone at two levels of fineness. Strengths of mortar cubes were tested at 1, 3, 7, and 28 d and statistical analysis was performed with a 95% confidence level. Additionally, LC^3 pastes were analyzed using x-ray diffraction, mercury intrusion porosimetry, scanning electron microscopy, and isothermal calorimetry. The fineness of the calcined clay along with the fineness of limestone is found to be statistically significant for 28-d strength in LC^3 mortars made with kaolinitic and montmorillonite calcined clays. All hydrated blends had a hemicarboaluminate phase, whose intensity was related to the fineness of the calcined clay, and the monocarboaluminate phase formation was found to be dependent on both the fineness and type of calcined clay. Porosimetry revealed that LC^3 pastes with illite clay have larger threshold pore diameters than those with kaolinite clay. LC^3 pastes containing kaolinite have denser microstructures due to C–S–H and hemicarboaluminate formation. Pastes produced with coarse calcined clay and coarse limestone led to a broader, weaker heat development peak and lower normalized cumulative heat. LC^3 with kaolinitic clay has the highest normalized cumulative heat, while that with montmorillonite calcined clay has the lowest.

M. Atasever (✉) · S. T. Erdoğan
Department of Civil Engineering, Middle East Technical University, Ankara 06800, Turkey
e-mail: muhammet.atasever@agu.edu.tr

S. T. Erdoğan
e-mail: sinante@metu.edu.tr

Present Address:
M. Atasever
Department of Civil Engineering, Abdullah Gul University, Kayseri 38080, Turkey

Graphical abstract

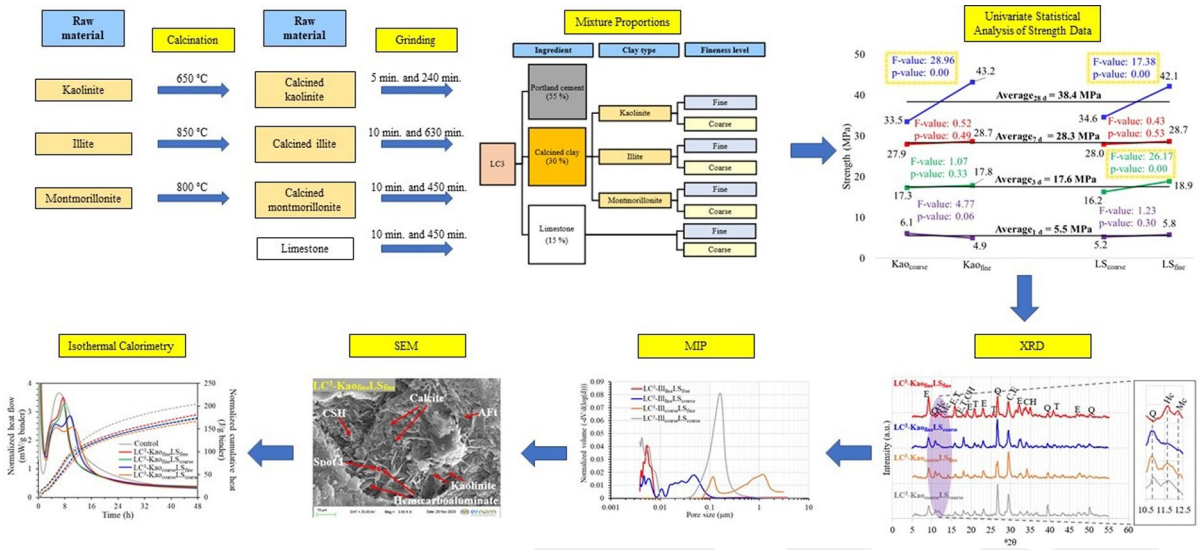

Keywords Limestone calcined clay cement · Kaolinite · Illite · Montmorillonite · Fineness

1 Introduction

Cement industry activities are estimated to contribute 5–7% of global man-made CO_2 emissions [1–4]. Supplementary cementitious materials (SCMs) have been used by the cement industry to reduce CO_2 emissions for many years [5–9]. However, since Portland cementitious systems cannot incorporate high amounts of SCMs without compromising mechanical properties, and because SCM properties vary by region, the search for alternative binders has intensified. One such binder is limestone calcined clay cement (LC^3). LC^3 boasts lower CO_2 emissions and cost compared to Portland cement, due to its significantly lowered clinker content. Beyond ~ 7 d, its mechanical properties mirror those of Portland cement. Furthermore, it can be produced using equipment and materials already present in existing cement factories [10–12]. Typical LC^3 comprises 50% Portland cement clinker, 30% calcined clay, 15% limestone, and 5% gypsum [13, 14]. Its mechanical performance, as well as its mineralogical and calorimetric properties, are related to the type and grade of calcined clay used in the binder, and the fineness of the components that make up LC^3 [15, 16]. Common types of clay found in the earth's crust include kaolinite, illite, and montmorillonite [17]. Calcination or thermal activation is the predominantly adopted method for increasing the reactivity of clays [18–21]. When thermal activation is applied, the pozzolanic activity of these minerals ranks, from highest to lowest, as kaolinite, montmorillonite, and illite [15]. Mechanical activation has gained attention in recent years as an effective method for activating illitic or montmorillonite clays. In addition to its lower energy requirement compared to calcination, mechanical activation can amorphize the structure of illitic and montmorillonite clays, a feat that most thermal activation methods cannot achieve [22–24]. Since kaolinite is richer in aluminosilicates than the other two clay minerals, most studies on LC^3 have concentrated on utilizing kaolinite of various grades [10, 16, 25–27]. Notably, after 7 d, LC^3-50 mortars, which incorporated calcined clays with at least 41.9% kaolinite, demonstrated mechanical properties comparable to those of Portland cement mortars [20]. This performance might be attributed to the formation of calcium silicate hydrate, resulting from the reaction of metakaolin with portlandite, and to the generation of carboaluminate phases, namely hemicarboaluminate and monocarboaluminate [28]. These phases develop through the interaction of alumina in C_3A with both portlandite and limestone. In LC^3, a similar reaction takes place, which involves an

interaction among the reactive aluminosilicate phases derived from metakaolin, calcium carbonate from limestone, and portlandite from Portland cement. The fineness of the constituents directly affects the hydration degree of cementitious systems [29, 30]. A recent study [16] investigated the impact of two different fineness levels of each component of a typical LC^3 mix, which included calcined clay (with less than 50% kaolinite), limestone, and cement. The study found that while clinker and calcined clay fineness can impact strength at all ages, limestone fineness significantly impacts only the early-age strength.

Current literature reveals a gap in studies that compare different clay types with significantly varied levels of fineness, aiming to highlight the critical role of component fineness in LC^3. Moreover, these studies lack substantiation of their findings through comprehensive statistical analysis. To address this gap, the design of the study focuses on evaluating the performance of LC^3, paying special attention to two distinct fineness levels of calcined clay and limestone. Consequently, three distinct types of calcined clays (kaolinite, illite, and montmorillonite) were carefully selected. The impact of the fineness of these clays and limestone on compressive strength was evaluated using univariate statistical analysis. Additionally, the study investigates the influence of component fineness in LC^3 on the mineralogical, morphological, and hydration characteristics.

2 Materials and methods

2.1 Materials

The LC^3 blends were prepared in a laboratory by mixing Portland cement (PC) clinker, limestone (LS), gypsum, and various calcined clays. These clays included kaolinite clay (Kao, from Zafer Mining, Balıkesir), illite clay (Ill, from Baştaş Cement Plant, Ankara), and montmorillonite clay (Mont, from Votorantim Cement Plant, Ankara). The chemical composition of the raw materials was determined using x-ray fluorescence spectroscopy (XRF, Rigaku ZSX Primus II), and their various physical properties are presented in Table 1.

Figure 1 shows the x-ray diffraction (XRD) patterns for the starting materials. Their mineral phase compositions were determined through Rietveld refinement using MAUD [31], as shown in Fig. 2.

Figure 3 showcases the Blaine fineness of the materials and the grinding duration required to achieve the desired levels of fineness. The order of hardness of the LC^3 mineral admixtures used in this study appears to be Ill > Mont > LS > Kao, consistent with findings from prior research [32].

Prior to milling, 5 kg of material was dried at 110 °C for each run. The ball mill, measuring 465 mm in length and 370 mm in diameter, had a volume of ~ 50 dm^3. The milling media consisted of 15 hard steel balls of 50 mm diameter, 62 balls of 40 mm, 174 balls of 29 mm, 160 balls of 22 mm, and 210 cylpebs of 16 mm length, totaling 621 balls with a combined mass of ~ 57 kg, as described in [33]. The milling process, conducted using this laboratory ball mill, was performed at a rotation speed of

Table 1 Oxide composition and physical properties of materials used

Oxide (%)	PC clinker	Kao	Ill	Mont	LS	Gypsum
CaO	65.8	0.2	2.1	3.7	53.5	37.3
SiO_2	20.7	55.2	51.3	61.5	1.1	0.6
Al_2O_3	5.2	30.1	23.4	14.3	0.4	0.2
Fe_2O_3	3.0	0.7	7.7	8.6	0.2	0.1
MgO	1.8	0.1	2.9	2.6	0.4	0.2
K_2O	0.7	0.8	4.7	1.6	0.1	0.0
SO_3	1.2	2.9	0.5	0.1	0.1	47.0
Na_2O	0.4	–	1.1	0.3	–	–
Loss on ignition	1.2	10.0	6.3	7.3	44.2	14.6
Density (g/cm^3)	3.11	2.63	2.72	2.63	2.72	2.51

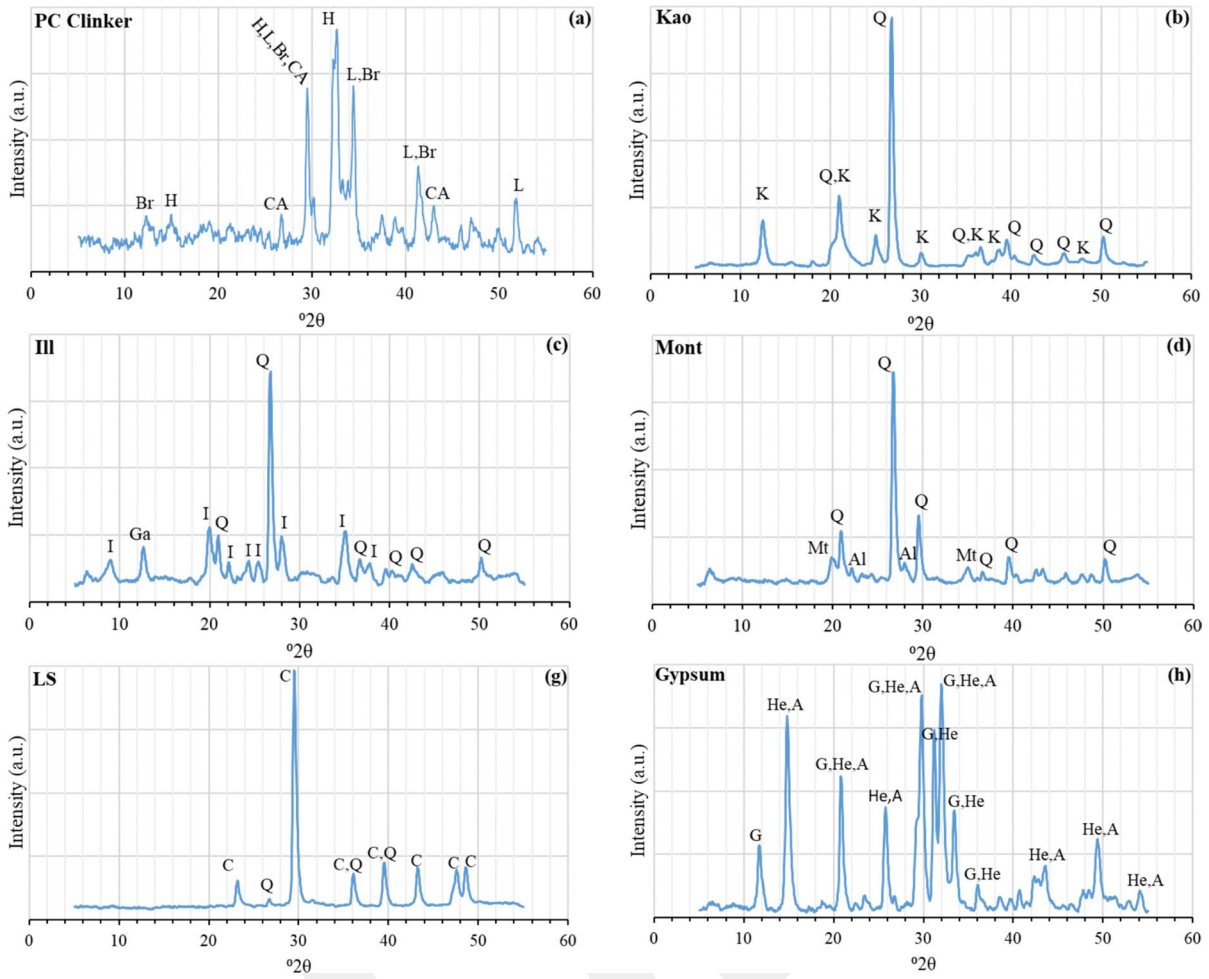

Fig. 1 XRD patterns for: **a** PC clinker, **b** Kao, **c** Ill, **d** Mont, **e** LS, **f** Gypsum (Legend: K-Kaolinite; Q-Quartz; I-Illite; Ga-Garronite; Mt-Montmorillonite; C-Calcite; Al-Albite; G-Gypsum; He-Hemihydrate; A-Anhydrite)

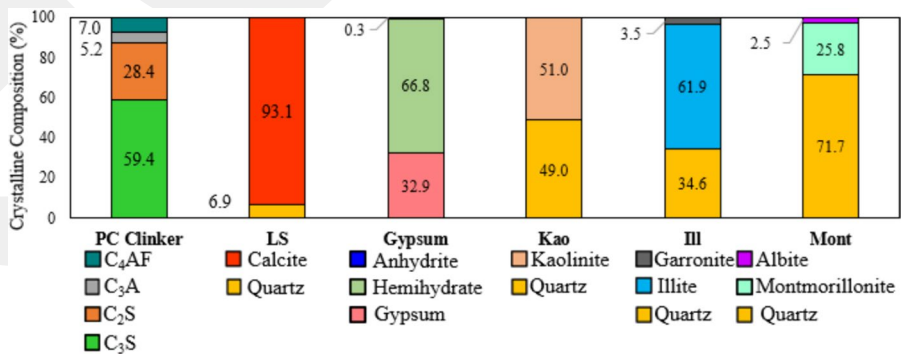

Fig. 2 Phase compositions of the materials used

70 rpm. After the clays were ground, they underwent a calcination process. The optimum calcination temperatures for each type of clay were determined based on the strength activity index (SAI) test, following the specifications outlined in ASTM C311 [34]. SAI is defined as the ratio of the compressive strength of

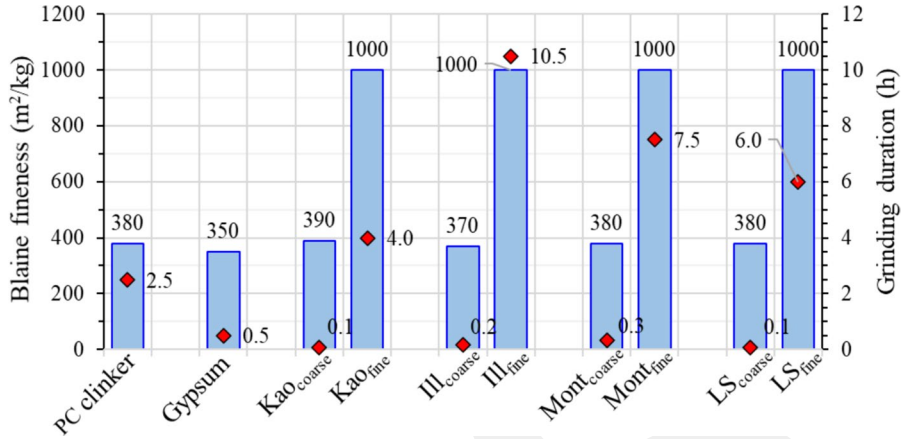

Fig. 3 Blaine fineness of the materials used and corresponding grinding durations

mortar incorporating 20% by mass of the calcined clay in the binder to the strength of the control mortar without any clay. A higher SAI indicates higher activity of the calcined clay. In determining the optimal calcination temperature, SAI was determined for clays calcined at every 50 °C increment between 600 and 900 °C. All the clays were heated at 5 °C/min, held at the target temperature for 3 h, and then cooled naturally in the furnace. The results indicated that the optimum calcination temperatures were 650 °C for Kao, 850 °C for Ill, and 600 °C for Mont. Although "optimum" temperatures reported in the literature for clays seem to vary, similar thermal activation temperatures have been reported for Kao [35, 36], Ill [37, 38], and Mont [39, 40]. However, it is important to note that the optimum calcination temperature is influenced by various factors, including the type of calcination (flash or static), the fineness of the clay being calcined, the amount of each mineral (kaolinite, illite, or montmorillonite), and the impurities present in the clay [41, 42].

2.2 Mix design

The gypsum content of the PC control mixture, needed to regulate the setting of the PC clinker, was determined using strength tests as outlined in ASTM C 563 [43], resulting in a PC gypsum:clinker ratio of 5:95. For LC^3 containing 30% calcined clay and 15% limestone, the gypsum:clinker ratio was increased slightly and set as 3:52. The ratio used here is lower than in the literature that attempt to achieve a "sulfate balance" or to increase strength. The "proper" amount of added gypsum in LC^3 depends on many factors, including SCM fineness and chemical composition. The use of calorimetry curves have been proposed to identify this amount [44, 45]. The decision to use a low amount of added gypsum allows the investigation of the effect of clay type and fineness and of limestone fineness on the sulfate need of the system. The samples were labeled according to the following convention: "LC^3-Calcined Clay $Type_{Calcined\ Clay\ Fineness}$-$Limestone_{Limestone\ Fineness}$". Table 2 gives the Blaine finenesses chosen for the powder components of the different mixtures.

2.3 Test methods

Mortars were prepared using silica sand in accordance with ASTM C305 [46], with a water-to-binder ratio of 0.48 and a flow of 110 ± 5%, achieved by adjusting the superplasticizer content as specified by ASTM C1437 [47]. The LC^3 blends incorporated a superplasticizer (Sikament FFN) with a density of 1.15–1.19 kg/l at 20 °C. The amount of superplasticizer varied depending on the fineness of the calcined clays and limestone, with 1.5% by weight of cement used when both materials were fine, 1.3% when calcined clays were fine and limestone was coarse, and 1.0% when calcined clays were coarse, and limestone was fine. No superplasticizer was used when both materials were coarse. Strength development of these mortars was evaluated in accordance with ASTM C109 [48], using 50 mm cubes. After being removed from their molds, the mortar cubes underwent a curing process in water at room temperature (23 ± 2 °C) until reaching specified test age (1, 3, 7, and 28 d). The microstructures of the hardened LC^3 pastes were

Table 2 Finenesses chosen for the components in the LC^3 blends

Mixture ID	Blaine fineness (m^2/kg)					
	PC	Kao	Ill	Mont	LS	Gypsum
Control	380	–	–	–	–	350
LC^3-$Kao_{fine}LS_{fine}$	380	1000	–	–	1000	
LC^3-$Kao_{fine}LS_{coarse}$	380	1000	–	–	380	
LC^3-$Kao_{coarse}LS_{fine}$	380	390	–	–	1000	
LC^3-$Kao_{coarse}LS_{coarse}$	380	390	–	–	380	
LC^3-$Ill_{fine}LS_{fine}$	380	–	1000	–	1000	
LC^3-$Ill_{fine}LS_{coarse}$	380	–	1000	–	380	
LC^3-$Ill_{coarse}LS_{fine}$	380	–	370	–	1000	
LC^3-$Ill_{coarse}LS_{coarse}$	380	–	370	–	380	
LC^3-$Mont_{fine}LS_{fine}$	380	–	–	1000	1000	
LC^3-$Mont_{fine}LS_{coarse}$	380	–	–	1000	380	
LC^3-$Mont_{coarse}LS_{fine}$	380	–	–	380	1000	
LC^3-$Mont_{coarse}LS_{coarse}$	380	–	–	380	380	

investigated using scanning electron microscopy (SEM) coupled with energy dispersive x-ray (EDX) composition analysis (Zeiss Evo LS10). For the SEM analysis, paste samples were prepared following the mixing procedure outlined in ASTM C 305 and cured in water at room temperature until the day of testing. The 28-day bulk paste samples were examined at magnifications of 250× and 3000×. Additionally, 28-day bulk paste samples, prepared according to the same mixing procedure as the SEM analysis, were used for the mercury intrusion porosimetry (MIP, Quantachrome Poremaster 60) analysis. Pore size distribution was determined using a maximum pressure of 375 MPa. XRD analysis (Olympus BTX-II) was conducted in the range of 5–55°2θ with a resolution of 0.25°2θ at room temperature (23 ± 2 °C). For the XRD analysis of raw materials, no curing was applied, whereas for the hardened paste samples, the tests were prepared in accordance with ASTM C 305 and cured in water at room temperature (23 ± 2 °C) until the day of testing. On the testing day, the hardened paste samples were ground, and their microstructure was examined under the specified initial settings. The heat evolution of pastes was measured using an isothermal calorimeter (TAM Air, TA Instruments). Consequently, 10 g paste samples were prepared at room temperature (23 ± 2 °C) and subsequently loaded into the device. The hydration kinetics of the paste samples were monitored for up to 48 h.

3 Results and discussion

3.1 Strength development

Figure 4a, c, and e depict the strength development of LC^3 produced using combinations of fine or coarse ingredients, Kao/LS, Ill/LS, and Mont/LS, up to 28 d. Meanwhile, Fig. 4b, d, and f show both the main effect plot and statistical outputs (i.e. F-value and p-value) for calcined clay and LS, considering two different fineness levels for the aforementioned test ages. The main effect plot represents the mean responses corresponding to each level of an independent variable, thereby illustrating the impact of these variables on the dependent variable within the context of an experiment.

The 1-d and 3-d strength of LC^3 mortars prepared using various clays are similar irrespective of the clay type and its fineness. However, strengths at 7 d and 28 d reveal that the clay type directly influences the performance of LC^3. The difference in performance can be attributed to the distinct structural characteristics of the clays. For instance, kaolinite has a 1:1 structural layer, while illite and montmorillonite feature a 2:1 structural layer. Kaolinite has more OH groups in unique positions within its structure compared to illite and montmorillonite, leading to a unique decomposition that reduces crystallinity significantly, making it more reactive at later ages. Conversely, in illite and montmorillonite, the O^{2-} groups from one layer align

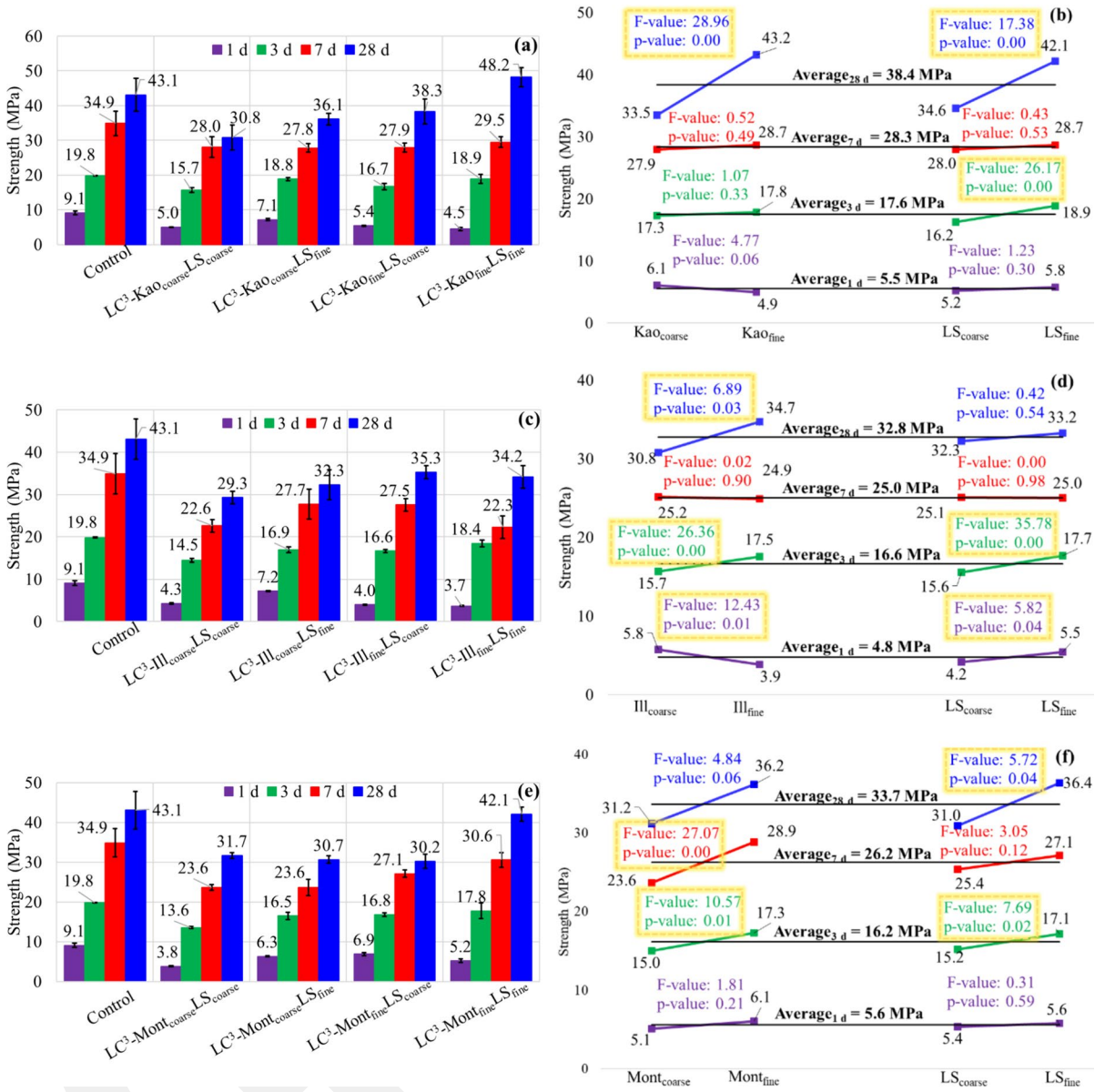

Fig. 4 Strength development (**a**, **c**, **e**), and main-effect plots and statistical results (**b**, **d**, **f**) for LC^3 mixtures produced with fine and/or coarse Kao/LS, Ill/LS, and Mont/LS

next to those of another layer, leading to fewer OH ions being released into the solution. Additionally, the structure of these minerals features an octahedral alumina sheet encased between two silicon tetrahedron sheets. Consequently, illite and montmorillonite are less reactive than kaolinite [15].

The main effect plots in Fig. 4b, d, and are utilized to analyze the differences in strength from the mean strength at different levels of the fine/coarse factor, represented by a line. A horizontal line indicates the absence of a main effect. Slight deviations from the horizontal line may significantly impact the response. A steeper slope signifies a greater magnitude of the main effect. The p-values helps interpret the significance of the result. For a confidence level of 95%, a p-value greater than 0.05 suggests that the result is not significant. A p-value less than 0.05 indicates significance, a value less than 0.01 denotes

high significance, and so on [49]. Based on this information, whenever the fineness of clay or limestone at various ages is statistically significant, the corresponding F-value and p-value for these materials are highlighted with a yellow dashed rectangle. Figure 4b shows that in LC^3-Kao-LS, the impact of Kao fineness on 28-d strength, and that of LS at 3 and 28 d, is statistically significant. The statistical significance of Kao fineness in the 28-d strength could be linked to the aluminate content and the structural layer of kaolinite. Meanwhile, the 1:1 structural layer of kaolinite fosters a more alkaline environment by releasing additional OH^- ions into the cementitious matrix, as reported in [15, 50]. On the other hand, the statistical significance of LS fineness in LC^3-Kao-LS on 3- and 28-d strengths is attributed to the filler effect of LS at 3 d and its role in forming carboaluminate phases at 28 d. Figure 4d shows that the fineness of Ill significantly affects strength at 1 d, 3 d, and 28 d, while the fineness of LS influences strength at 1 d and 3 d in LC^3-Ill-LS. Interestingly, coarser Ill resulted in higher 1-d strength compared to its finer counterpart. This phenomenon was also observed in LC^3 mixtures made with Kao, though the effect of Kao fineness on 1-d strength in LC^3-Kao-LS did not reach statistical significance. In LC^3 mixtures containing Kao and Ill, the result is linked to sulfate content. As reported by [51, 52], the sulfate requirement in cementitious mixtures is determined by their aluminate content. Therefore, the addition kaolinite, which is rich in aluminate, calls for adjusting the sulfate levels. Incorporating additional gypsum into the LC^3 may slow down the hydration of aluminate components but improves that of silicate components, highlighting the pivotal role of gypsum in early-age strength. Consequently, in LC^3 mixes with coarse Kao and Ill, lower sulfate demand for finer cases results in higher 1-d strength compared to mixes with finer Kao and Ill. Similar observations have been reported in other studies [53]. The statistical significance of Ill fineness in the 3- and 28-d strengths of LC^3-Ill-LS is attributed to its inert nature and resulting physical effects, such as cement dilution, dispersion, and nucleation. This inert characteristic of Ill is further indicated by the lack of statistical significance in LS fineness, suggesting a limited interaction among Ill, LS, and Portland cement at 28 d. Figure 4f shows that the effect of the fineness of Mont and LS on strength of LC^3-Mont-LS is statistically significant at different intervals: Mont at 3 d and 7 d, and LS at 3 d and 28 d. The significance of Mont fineness for strength at early ages might be due to the nucleation and filling effect of Mont. Although montmorillonite shows greater pozzolanic activity than illite, the statistical insignificance of Mont fineness for strength at later ages could be related to with the low amount of montmorillonite in this clay (Fig. 2).

3.2 Mineralogical changes

The 28-d XRD curves for LC^3 pastes prepared with clays and limestone of varying fineness are shown in Fig. 5.

Figure 5 demonstrates that hemicarboaluminate which refines the pore structures and contributes to strength development [25, 28, 54], formed in all mixtures, regardless of the type of calcined clay used. However, in mixtures containing finer limestone, its intensity is more prominent. Both monocarboaluminate and hemicarboaluminate were observed in LC^3-$Kao_{fine}LS_{fine}$ and LC^3-$Kao_{coarse}LS_{fine}$ (Fig. 5a). The conversion of hemicarboaluminate to monocarboaluminate in these mixtures occurred at 28 d, driven by the higher aluminate content in Kao compared to other calcined clays, the structural layer of kaolinite in Kao, and the influence of particle size of LS. Figure 5b illustrates that the greater amounts of hemicarboaluminate form in LC^3-Ill-LS mixtures with fine LS than in mixtures with coarse LS. The fineness of Ill does not significantly impact the formation of hemicarboaluminate. This observation is also corroborated by the statistically insignificant strength of LS at 28 d in Fig. 4d. Figure 5c indicates that hemicarboaluminate in LC^3-$Mont_{fine}LS_{coarse}$ is greater than in LC^3-$Mont_{coarse}LS_{coarse}$. This suggests that Mont might be a significant aluminum source for LS. Several studies have highlighted that while montmorillonite possesses a 2:1 structural layer like illite, it is inherently less stable and may provide greater amounts of aluminum. Consequently, montmorillonite emerges as a more reactive component in LC^3 [15, 55].

3.3 Pore size distribution and porosity

The pore structures of 28-d-old LC^3 pastes determined with MIP are presented in Fig. 6.

The LC^3 pastes made with coarse calcined clay, typically exhibit the highest porosity, regardless of

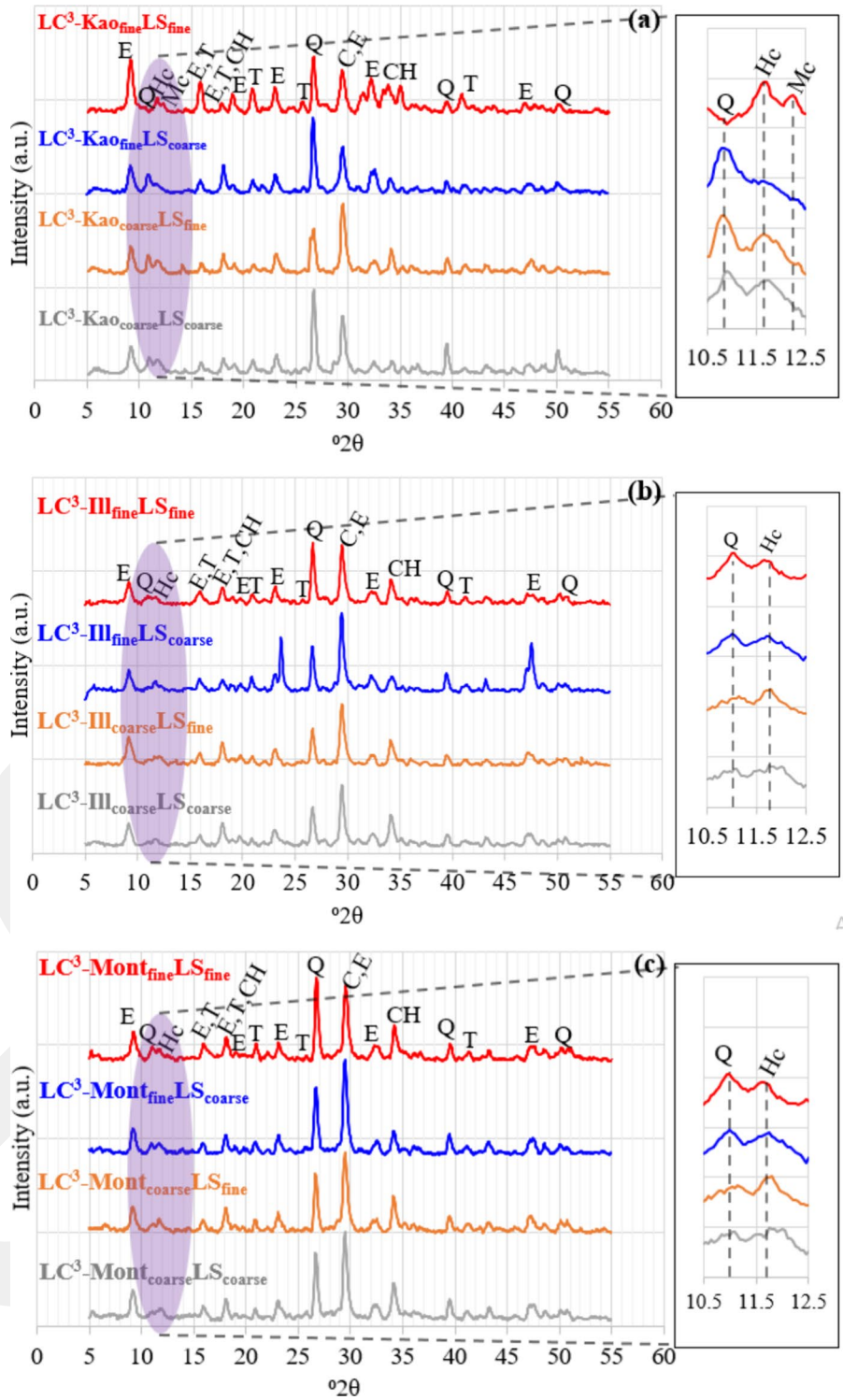

Fig. 5 28-d XRD patterns of LC^3 pastes produced with fine and/or coarse: **a** Kao/LS, **b** Ill/LS, **c** Mont/LS (Legend: E-ettringite; Hc-hemicarboaluminate; Mc-monocarboaluminate; T-Tobermorite; CH-Portlandite; Q-Quartz; G-Gypsum; C-Calcite)

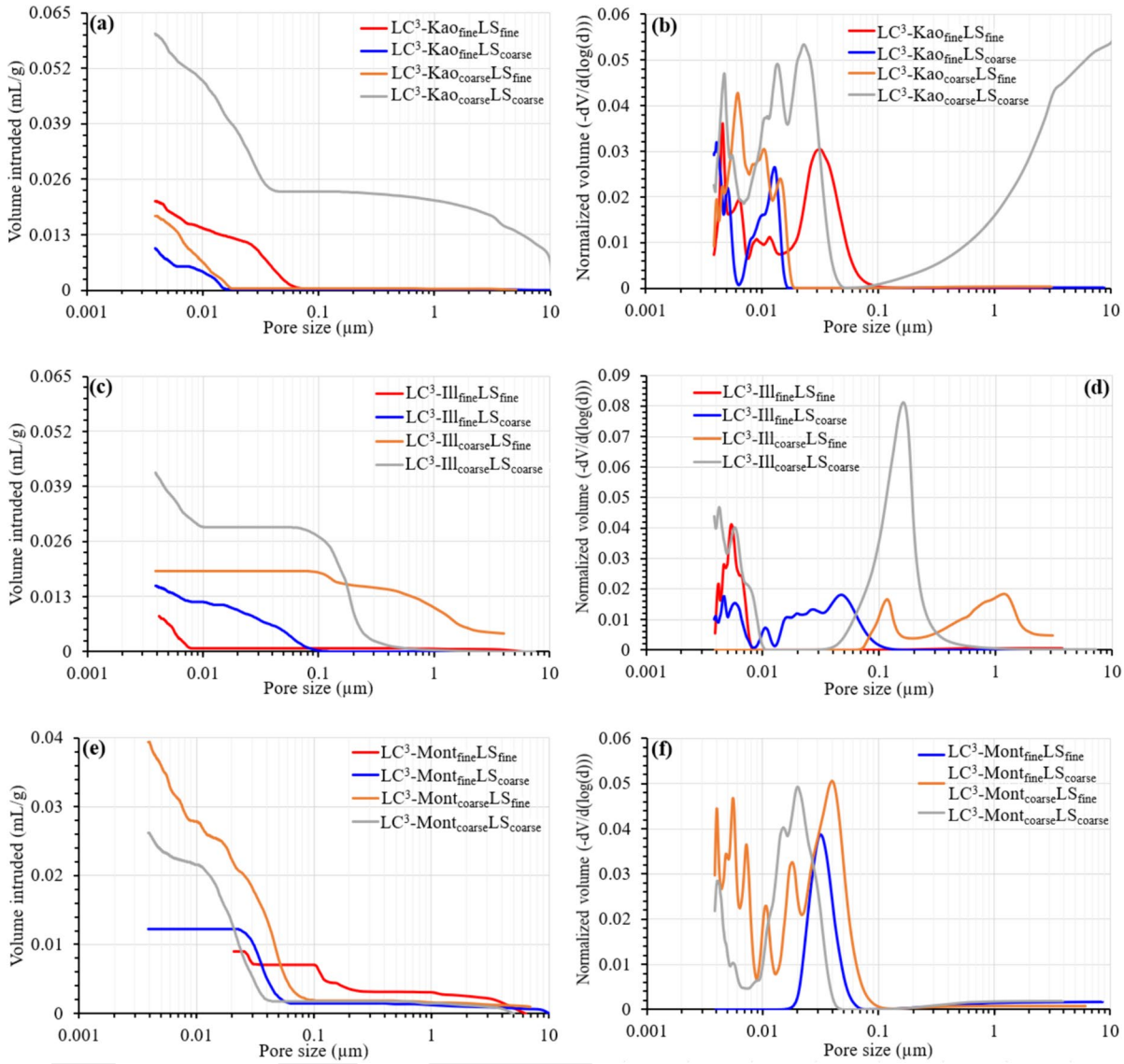

Fig. 6 Volume intruded and pore size distribution curves for 28-d LC^3 pastes: **a**, **b** LC^3-Kao-LS; **c**, **d** LC^3-Ill-LS; **e**, **f** LC^3-Mont-LS

the type of clay used (Fig. 6a, c, and e). The pore size distribution confirmed the predominant presence of capillary pores (0.005–5 μm) across all samples. In the coarse samples of LC^3-Kao and LC^3-Ill, larger pores (> 1 μm) were primarily observed, potentially due to less effective compaction. In contrast, the fine cases of LC^3-Kao and LC^3-Ill exhibited fewer large pores and a higher concentration of capillary pores in the 0.010–0.1 μm range. Both fine and coarse ingredient cases of LC^3-Mont displayed significant amounts of capillary pores, with the coarse case showing a slightly higher presence of larger pores compared to the fine ones. Comparing the threshold pore diameters of the pastes, the largest pore size at which the volume of mercury intruded increases significantly [56], the differences are noted depending on the type of calcined clay used. Specifically, for Kao, the threshold pore diameters range from 0.02 to 0.06 μm; for Ill, they vary from 0.008 to 1.8 μm; and for Mont, they extend from 0.03 to 0.1 μm. Assessment of the threshold diameter and normalized volume reveals differences in strength by highlighting the differences

in quantities of large and small pores within the samples. Even though LC^3-$Kao_{fine}LS_{fine}$ has the highest strength without having the smallest threshold diameter, the varying pore sizes in other mixtures account for their lower strengths.

3.4 Microstructure characterization

Figure 7, 8, and 9 illustrate the effect of calcined clay and limestone fineness on the microstructures of LC^3. Figure 7a–e shows the impact of Kao_{fine}/

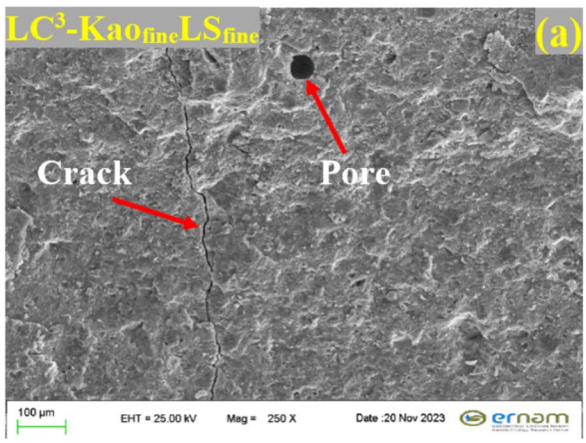

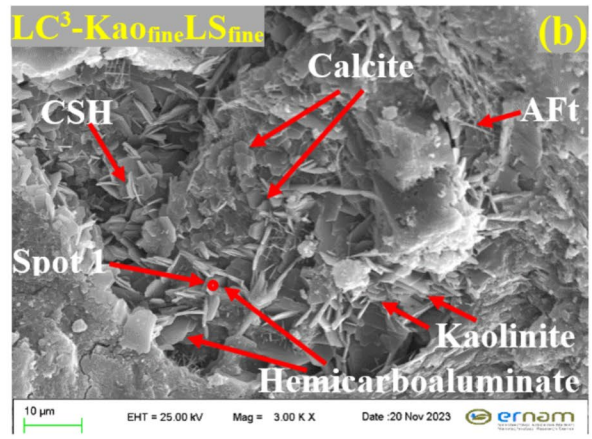

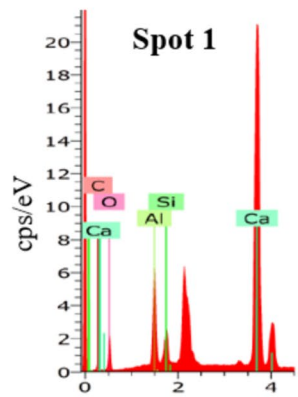

(c)

Element	Atomic (%)
Ca	46.5
O	33.5
Al	10.3
C	5.2
Si	4.6

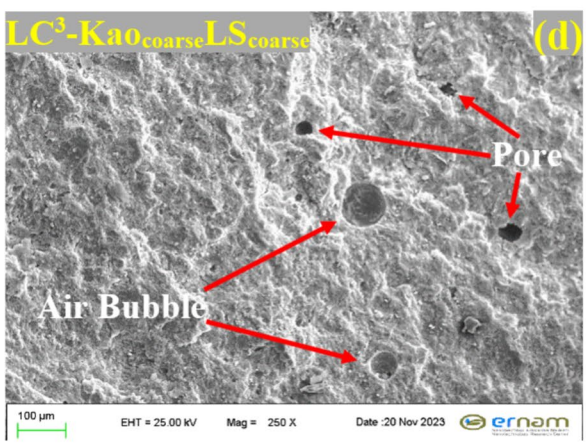

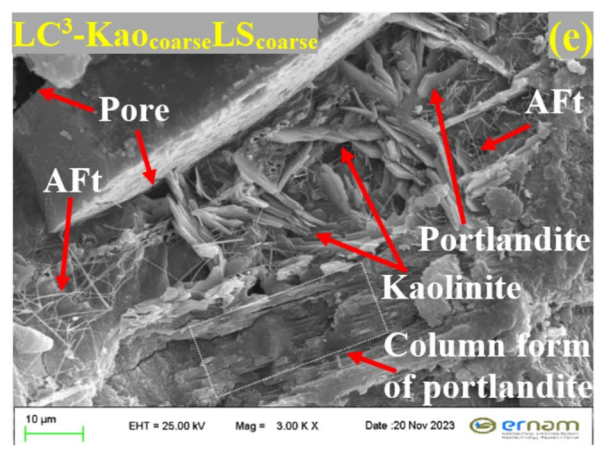

Fig. 7 SEM/EDX micrographs of 28-d pastes: **a**, **b** LC^3-$Kao_{fine}LS_{fine}$; **c** EDX result of Spot 1 in (**b**); **d**, **e** LC^3-$Kao_{coarse}LS_{coarse}$

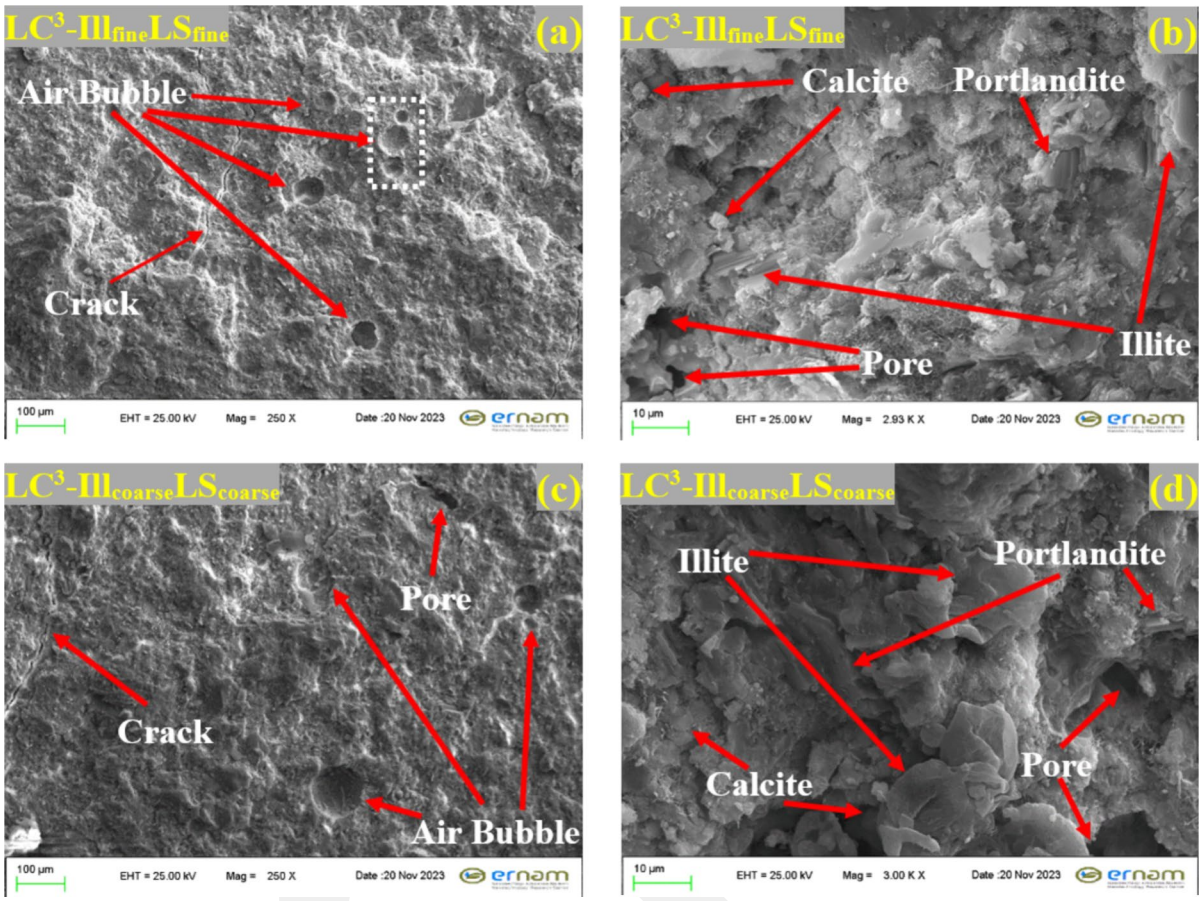

Fig. 8 SEM micrographs at 28 d: **a**, **b** LC^3-$Ill_{fine}LS_{fine}$, **c**, **d** LC^3-$Ill_{coarse}LS_{coarse}$

Kao_{coarse} and LS_{fine}/LS_{coarse} on the microstructures of LC^3. LC^3-$Kao_{fine}LS_{fine}$ matrix, rich in amorphous CSH gel and with minimal portlandite, contrasts with LC^3-$Kao_{coarse}LS_{coarse}$. This difference stems from pozzolanic reaction that fills voids and enhances the microstructure. Despite the identification of needle-like ettringite structures in Fig. 7b and e, the observed densification of the microstructure in Fig. 7b may be predominantly attributed to the concurrent formation of CSH and hemicarboaluminate. This is confirmed by the EDX analysis of the hexagonal particles with smooth surfaces in Fig. 7b and e, which suggests they may be a poorly crystallized kaolinitic phase, in alignment with the clay mineral images in [57, 58]. The labeling of this mineral as hemicarboaluminate rather than calcium hydroxide is related to the amount of aluminum observed in the EDX analysis. Additionally, the presence of hemicarboaluminate in the 28-d XRD results further supports the identification of this mineral as hemicarboaluminate. The abundance of kaolinite in Fig. 7e relative to Fig. 7b might imply a lower hydration degree in LC^3-$Kao_{coarse}LS_{coarse}$ compared to LC^3-$Kao_{fine}LS_{fine}$.

Figure 8 shows a pronounced presence of air voids in LC^3 pastes made with Ill. This situation is not fineness-specific, as it persists across different Ill fineness levels (fine and coarse) and is also evident at greater magnification (Fig. 8b and d). The simultaneous presence of portlandite and Ill suggests reduced pozzolanic activity of Ill. In effective pozzolanic reactions, products like C–S–H typically fill voids, resulting in a denser microstructure. A greater amount of voids may imply less efficient reactions leading to reduced strength, similar to [59]. The characterization of the irregular sheet-like shapes with rough surface morphology in Fig. 8b and d as illite, based on [60],

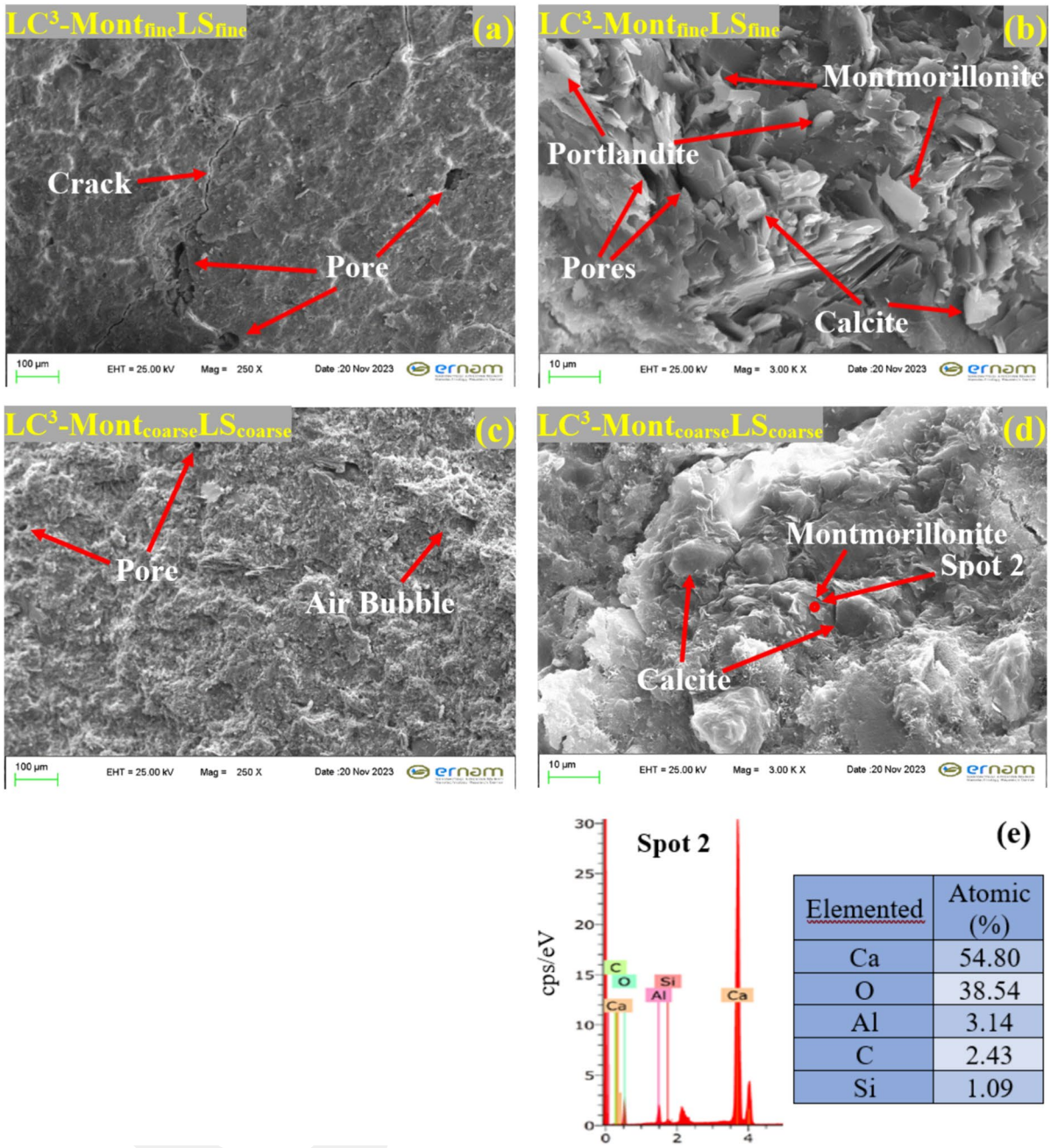

Elemented	Atomic (%)
Ca	54.80
O	38.54
Al	3.14
C	2.43
Si	1.09

Fig. 9 SEM/EDX micrographs at 28 d: **a**, **b** LC^3-Mont$_{fine}$LS$_{fine}$; **c**, **d** LC^3-Mont$_{coarse}$LS$_{coarse}$; **e** EDX result of Spot 2 in (**d**)

further supports the conclusion that LC^3 pastes incorporating Ill fail to develop a densified microstructural matrix.

The visibly microcracked microstructure in Fig. 9a contrasts notably with that of Fig. 9c, the disparity is attributed to the expansive properties of montmorillonite (detected by EDX analysis in Fig. 9e) and aligns with findings in previous studies [61, 62]. Figure 9b further reveals the presence of portlandite and calcite structures, indicating incomplete reaction of Mont. Moreover, the microstructural of LC^3-Mont$_{fine}$LS$_{fine}$ (Fig. 9b) reveals porous

formations resembling holes. This observation suggests a potential delay in the pozzolanic reaction of Mont particles, agreeing well with [63–65].

3.5 Heat evolution

The change in normalized heat flow and cumulative heat for the various pastes are systematically presented in Fig. 10.

A consistent observation across all samples is the occurrence of a marked exothermic reaction. The initial phase of this reaction, which lasts up to 30 min, is attributed to the wetting and dissolution processes characteristic of the paste composition. The second (alite) peak is directly related to the dissolution of C_3S and the subsequent precipitation of C-S–H. In this phase, sulfate is also adsorbed onto the C–S–H. This peak becomes much more prominent when calcined clay and limestone are integrated into the cementitious matrix. This can be observed from Fig. 10 if heat flow is normalized by the amount of clinker instead of total binder. Since LC^3 contains nearly half the amount of clinker in PC, the LC^3 curves need to be doubled leading to alite peak heights of 5.0–5.5 mW/g clinker compared with ~ 3.9 mW/g clinker peak height for the control. This increase is linked to the filler effect produced by these two SCMs [28]. This physical effect related with the increased surfaces provided by the fine materials promotes the accelerated nucleation of C–S–H and adsorption of sulfate ions from the pore solution [44, 66]. The alite peak also helps assess the sulfate balance in LC^3. Given a sufficient sulfate amount in LC^3, the aluminate peak (the third peak) invariably succeeds the alite peak [44, 45]. The alite peak emerges earlier in LC^3 produced with Kao compared to blends containing other clays, when the same clay/limestone fineness combinations are compared (Fig. 10a vs. Figure 10b or Fig. 10c). This suggests that gypsum is depleted more rapidly in LC^3 mixtures containing Kao and that the chemical composition of the calcined clay is a factor influencing the sulfate balance. The enhanced alite reaction results in a higher rate of C–S–H and ettringite precipitation, and consequently, earlier sulfate depletion [67]. Additionally, the time between the aluminate and alite peaks in LC^3 mixtures produced with Kao (compare

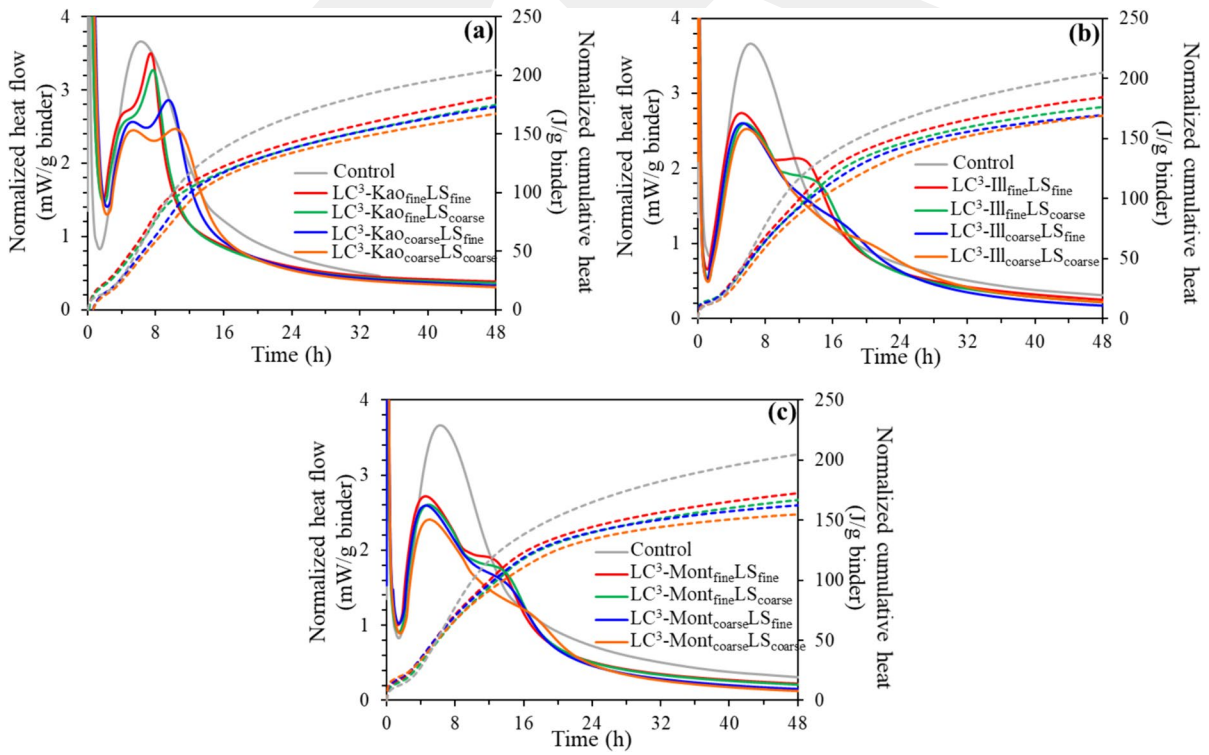

Fig. 10 Normalized heat flow and cumulative heat versus time for: **a** LC^3-Kao-LS; **b** LC^3-Ill-LS; **c** LC^3-Mont-LS

the curves in Fig. 10a) is shorter than in those produced with Ill and Mont. Considering that all pastes contain the same amount of gypsum, this indicates a higher gypsum need (sulfate demand) in Kao-containing mixtures. Kao also causes narrower aluminate peaks. Furthermore, the LC^3 paste produced with Kao_{coarse} has a longer time between these peaks than the paste produced with Kao_{fine}, showing the effect of SCM fineness on the sulfate need. Hence, LC^3 with Kao_{fine} requires a greater amount of gypsum than LC^3 with Kao_{coarse}. Similarly, LC^3-Kao_{coarse}-LS_{fine} requires more gypsum than LC^3-Kao_{coarse}-LS_{coarse}. However, the effect of LS fineness appears to be less significant than that of the Kao. This could also be related with the greater amount of calcined clay than limestone (30% and 15%) in LC^3. Similar effects of clay fineness and limestone fineness are also observed in Fig. 10b and c. LC^3 blends with Kao exhibit higher heat flow during the dormant period compared to those with Ill and Mont which also suggests more extensive sulfate consumption in kaolinite-rich mixtures. Comparing the total heat released by the different pastes, LC^3 blends produced with Kao achieve the highest cumulative heat at 48 h, due to combined hydration, pozzolanic reaction, and formation of carboaluminates. LC^3 blends with Mont registered the lowest heat. Although montmorillonite is generally more reactive than illite [15], the higher 48-h cumulative heat evolved by pastes containing Ill can be attributed to Ill containing ~ 62% illite but Mont containing only ~ 26% montmorillonite. Past studies [44, 45, 68, 69] offer mixed views on the impact of the calcined clay's chemical composition on the sulfate need of LC^3. The findings in this study suggest that both the fineness and chemical composition of the calcined clay influences the sulfate need of LC^3.

4 Conclusions

This study statistically examined the effects of particle size and type of calcined clay, along with limestone particle size, on the mechanical performance of LC^3, as well as their effects on morphology, mineralogy, and hydration kinetics. The following conclusions were reached:

- The fineness of kaolinitic clay significantly influences 28-d strength at a 95% confidence level, but its effect is not statistically significant at earlier ages. Similarly, the fineness of calcined illite clay is significant for late ages, yet does not enhance early strength. The effect of the fineness of these two clays on late strength relates to their structural layers and chemical compositions. The fineness of montmorillonite clay significantly affects strength at 3 and 7 d, while its impact on 1 and 28-d strength is not significant. This could be due to the low montmorillonite content in the clay used, mainly physically affecting hydration.
- Limestone fineness has a significant impact on 28-d strength of LC^3 blends containing calcined kaolinitic and montmorillonite clays but not in blends with illite clay. The interaction between limestone and calcined clay emphasizes the crucial role of the position of aluminates within the structural layers of clays.
- The hemicarboaluminate phase occurs in all LC^3 mixtures, independent of clay type; however, monocarboaluminate formation requires the fine grinding of kaolinitic clay and limestone. Unlike kaolinitic and montmorillonite clay, whose fineness significantly affects the hemicarboaluminate quantity, the fineness of illite clay has little impact.
- Clay type directly influences threshold pore diameter, with fineness playing a more crucial role in calcined clays of high activity and less so in those of low activity. Calcined clay fineness contributes to a denser microstructure more effectively than limestone fineness.
- The sulfate requirement in LC^3 mixtures is influenced more by the filler effect of calcined clays than by limestone. The aluminate peak intensity depends on the position of aluminum within the structural layer of calcined clay and its physical impact on the hydration of the cementitious system

Declarations

Conflict of interest The authors declare that they have no known competing financial interests or personal relationships that could have appeared to influence the work reported in this paper.

References

1. Turner LK, Collins FG (2013) Carbon dioxide equivalent (CO_2-e) emissions: a comparison between geopolymer and OPC cement concrete. Constr Build Mater 43:125–130. https://doi.org/10.1016/j.conbuildmat.2013.01.023
2. Maddalena R, Roberts JJ, Hamilton A (2018) Can Portland cement be replaced by low-carbon alternative materials? A study on the thermal properties and carbon emissions of innovative cements. J Clean Prod 186:933–942. https://doi.org/10.1016/j.jclepro.2018.02.138
3. Huntzinger DN, Eatmon TD (2009) A life-cycle assessment of Portland cement manufacturing: comparing the traditional process with alternative technologies. J Clean Prod 17(7):668–675. https://doi.org/10.1016/j.jclepro.2008.04.007
4. Gawah Q, Al-Osta MA, Maslehuddin M, Abdullah MA, Shameem M, Al-Dulaijan SU (2023) Development of sustainable self-compacting concrete utilising silico manganese fume. Eur J Environ Civ Eng 27(5):1897–1918. https://doi.org/10.1080/19648189.2022.2102083
5. Erdem TK, Meral Ç, Tokyay M, Erdoğan TY (2007) Use of perlite as a pozzolanic addition in producing blended cements. Cem Concr Compos 29(1):13–21. https://doi.org/10.1016/j.cemconcomp.2006.07.018
6. Knight KA, Cunningham PR, Miller SA (2023) Optimizing supplementary cementitious material replacement to minimize the environmental impacts of concrete. Cem Concr Compos 139:105049. https://doi.org/10.1016/j.cemconcomp.2023.105049
7. Malhotra VM, Hammings RT (1995) Blended cements in North America-a review. Cem Concr Compos 17(1):23–35. https://doi.org/10.1016/0958-9465(95)95757-Q
8. Hamdadou MN, Bignonnet F, Deboucha W, Ranaivomanana H, Leklou N, Arroudj K (2023) Hydration, mechanical and transfer properties of blended cement pastes and mortars prepared with recycled powder or limestone filler. J Build Eng 78:107541. https://doi.org/10.1016/j.jobe.2023.107541
9. Yong CL, Mo KH, Koting S, Ling TC (2024) Effect of various additives in activating early age properties of phosphorus furnace slag blended cement. J Build Eng 82:108136. https://doi.org/10.1016/j.jobe.2023.108136
10. Scrivener K, Martirena F, Bishnoi S, Maity S (2018) Calcined clay limestone cements (LC3). Cem Concr Res 114:49–56. https://doi.org/10.1016/j.cemconres.2017.08.017
11. Chaudhury R, Sharma U, Thapliyal PC, Singh LP (2023) Low-CO_2 emission strategies to achieve net zero target in cement sector. J Clean Prod 417:137466. https://doi.org/10.1016/j.jclepro.2023.137466
12. Schulze SE, Rickert J (2019) Suitability of natural calcined clays as supplementary cementitious material. Cem Concr Compos 95:92–97. https://doi.org/10.1016/j.cemconcomp.2018.07.006
13. Avet F, Li X, Scrivener K (2018) Determination of the amount of reacted metakaolin in calcined clay blends. Cem Concr Res 106:40–48. https://doi.org/10.1016/j.cemconres.2018.01.009
14. Sharma M, Bishnoi S, Martirena F, Scrivener K (2021) Limestone calcined clay cement and concrete: a state-of-the-art review. Cem Concr Res 149:106564. https://doi.org/10.1016/j.cemconres.2021.106564
15. Fernández R, Martirena F, Scrivener K (2011) The origin of the pozzolanic activity of calcined clay minerals: a comparison between kaolinite, illite and montmorillonite. Cem Concr Res 41(1):113–122. https://doi.org/10.1016/j.cemconres.2010.09.013
16. Vizcaíno Andrés LM, Antoni MG, Alujas Diaz A, Martirena Hernández JF, Scrivener K (2015) Effect of fineness in clinker-calcined clays-limestone cements. Adv Cem Res 27(9):546–556. https://doi.org/10.1680/jadcr.14.00095
17. Borno IB, Ashraf W (2023) Effects of co-calcining kaolinite-rich clay blends with alkali and alkali earth metal hydroxides. Appl Clay Sci 231:106742. https://doi.org/10.1016/j.clay.2022.106742
18. Zunino F, Scrivener K (2024) Reactivity of kaolinitic clays calcined in the 650 °C–1050 °C temperature range: towards a robust assessment of overcalcination. Cem Concr Res 146:105380. https://doi.org/10.1016/j.cemconcomp.2023.105380
19. Alujas A, Fernández R, Quintana R, Scrivener K, Martirena F (2015) Pozzolanic reactivity of low grade kaolinitic clays: influence of calcination temperature and impact of calcination products on OPC hydration. Appl Clay Sci 108:94–101. https://doi.org/10.1016/j.clay.2015.01.028
20. Bonavetti VL, Castellano CC, Irassar EF (2022) Designing general use cement with calcined illite and limestone filler. Appl Clay Sci 230:106700. https://doi.org/10.1016/j.clay.2022.106700
21. Zhou Y, Wang Z, Zhu Z, Chen Y, Wu K, Huang H, Anvarovna KG, Xu L (2022) Influence of metakaolin and calcined montmorillonite on the hydration of calcium sulphoaluminate cement. Case Stud Constr Mater 16:e01104. https://doi.org/10.1016/j.cscm.2022.e01104
22. Mañosa J, Alvarez-Coscojuela A, Marco-Gibert J, Maldonado-Alameda A, Chimenos JM (2024) Enhancing reactivity in muscovitic clays: mechanical activation as a sustainable alternative to thermal activation for cement production. Appl Clay Sci 250:107266. https://doi.org/10.1016/j.clay.2024.107266
23. Fitos M, Badogiannis EG, Tsivilis SG, Perraki M (2015) Pozzolanic activity of thermally and mechanically treated kaolins of hydrothermal origin. Appl Clay Sci 116–117:182–192. https://doi.org/10.1016/j.clay.2015.08.028
24. Tole I, Habermehl-Cwirzen K, Rajczakowska M, Cwirzen A (2018) Activation of a raw clay by mechanochemical process-effects of various parameters on the process efficiency and cementitious properties. Mater 11(10):1860. https://doi.org/10.3390/ma11101860
25. Avet F, Scrivener K (2018) Investigation of the calcined kaolinite content on the hydration of limestone calcined clay cement (LC3). Cem Concr Res 107:124–135. https://doi.org/10.1016/j.cemconres.2018.02.016
26. Chen Y, Zhang Y, Šavija B, Çopuroğlu O (2023) Fresh properties of limestone-calcined clay-slag cement pastes. Cem Concr Compos 138:104962. https://doi.org/10.1016/j.cemconcomp.2023.104962

27. Maraghechi H, Avet F, Wong H, Kamyab H, Scrivener K (2018) Performance of limestone calcined clay cement (LC3) with various kaolinite contents with respect to chloride transport. Mater Struct 51(5):125. https://doi.org/10.1617/s11527-018-1255-3
28. Zunino F, Scrivener K (2021) The reaction between metakaolin and limestone and its effect in porosity refinement and mechanical properties. Cem Concr Res 140:106307. https://doi.org/10.1016/j.cemconres.2020.106307
29. Dai J, Wang Q, Xie C, Xue Y, Duan Y, Cui X (2019) The effect of fineness on the hydration activity index of ground granulated blast furnace slag. Mater 12(18):2984. https://doi.org/10.3390/ma12182984
30. Lawrence P, Cyr M, Ringot E (2005) Mineral admixtures in mortars effect of type, amount and fineness of fine constituents on compressive strength. Cem Concr Res 35(6):1092–1105. https://doi.org/10.1016/j.cemconres.2004.07.004
31. Lutterotti L (2000) MAUD: a Rietveld analysis program designed for the internet and experiment integration. Acta Crystallogr Sect A Found Crystallogr 56:S54
32. Mañosa J, la Rosa JC, Silvello A, Maldonado-Alameda A, Chimenos JM (2023) Kaolinite structural modifications induced by mechanical activation. Appl Clay Sci 238:106918. https://doi.org/10.1016/j.clay.2023.106918
33. Ardoğa MK (2014) Effect of particle size on heat of hydration of pozzolan incorporated cements, MSc Thesis, Middle East Technical University, Türkiye
34. ASTM C311/C311M-22 (2022) Standard test methods for sampling and testing fly ash or natural Pozzolans for use in Portland-cement concrete, annual book of ASTM standards, ASTM International, West Conshohocken
35. Kassa AE, Shibeshi NT, Tizazu BZ (2022) Characterization and optimization of calcination process parameters for extraction of aluminum from Ethiopian kaolinite. Int J Chem Eng 2022:1–18. https://doi.org/10.1155/2022/5072635
36. Elimbi A, Tchakoute HK, Njopwouo D (2011) Effects of calcination temperature of kaolinite clays on the properties of geopolymer cements. Constr Build Mater 25(6):2805–2812. https://doi.org/10.1016/j.conbuildmat.2010.12.055
37. Garg N, Skibsted J (2016) Pozzolanic reactivity of a calcined interstratified illite/smectite (70/30) clay. Cem Concr Res 79:101–111. https://doi.org/10.1016/j.cemconres.2015.08.006
38. He C, Makovicky E, Øsbæck B (1995) Thermal stability and pozzolanic activity of calcined illite. Appl Clay Sci 9(5):337–354. https://doi.org/10.1016/0169-1317(94)00033-M
39. Seiffarth T, Hohmann M, Posern K, Kaps C (2013) Effect of thermal pre-treatment conditions of common clays on the performance of clay-based geopolymeric binders. Appl Clay Sci 73:35–41. https://doi.org/10.1016/j.clay.2012.09.010
40. Garg N, Skibsted J (2019) Dissolution kinetics of calcined kaolinite and montmorillonite in alkaline conditions: evidence for reactive Al(V) sites. J Am Ceram Soc 102(12):7720–7734. https://doi.org/10.1111/jace.16663
41. Ferreiro S, Canut MMC, Lund J, Herfort D (2019) Influence of fineness of raw clay and calcination temperature on the performance of calcined clay-limestone blended cements. Appl Clay Sci 169:81–90. https://doi.org/10.1016/j.clay.2018.12.021
42. Zunino F, Boehm-Courjault E, Scrivener K (2020) The impact of calcite impurities in clays containing kaolinite on their reactivity in cement after calcination. Mater Struct 53(2):44. https://doi.org/10.1617/s11527-021-01654-5
43. ASTM C563-20 (2020) Standard guide for approximation of optimum SO3 in hydraulic cement, annual book of ASTM standards, ASTM International, West Conshohocken
44. Zunino F, Scrivener K (2019) The influence of the filler effect on the sulfate requirement of blended cements. Cem Concr Res 126:105918. https://doi.org/10.1016/j.cemconres.2019.105918
45. Canbek O, Szeto C, Washburn NR, Kurtis KE (2023) A quantitative approach to determining sulfate balance for LC3. Cem 12:100063. https://doi.org/10.1016/j.cement.2023.100063
46. ASTM C305-20 (2020) Standard practice for mechanical mixing of hydraulic cement pastes and mortars of plastic consistency, annual book of ASTM standards, ASTM International, West Conshohocken
47. ASTM C1437-20 (2020) Standard test method for flow of hydraulic cement mortar, annual book of ASTM standards, ASTM International, West Conshohocken
48. ASTM C109/109M (2020) Standard test method for compressive strength of hydraulic cement mortars (Using 2-in. or cube specimens), Annual Book of ASTM standards, ASTM International, West Conshohocken, PA
49. Batool F, Prasad NGN, Bindiganavile V (2018) Statistical modeling of thermal conductivity for cement-based foam. J Build Eng 19:449–458. https://doi.org/10.1016/j.jobe.2018.05.022
50. Miranda-Trevino JC, Coles CA (2003) Kaolinite properties, structure and influence of metal retention on pH. Appl Clay Sci 23(1–4):133–139. https://doi.org/10.1016/S0169-1317(03)00095-4
51. Chen Y, Zhang Y, He S, Liang X, Schlangen E, Çopuroğlu O (2023) Improving structural build-up of limestone-calcined clay-cement pastes by using inorganic additives. Construct Build Mater 392:131959. https://doi.org/10.1016/j.conbuildmat.2023.131959
52. Bhavani S, Prasad MLV (2023) Strength and durability properties of SCC developed using limestone calcined clay cement (LC3). Mater Today Proc. https://doi.org/10.1016/j.matpr.2023.04.497
53. Briki Y, Zajac M, Ben Haha M, Scrivener K (2021) Impact of limestone fineness on cement hydration at early age. Cem Concr Res 147:106515. https://doi.org/10.1016/j.cemconres.2021.106515
54. Bahhou A, Taha Y, Hakkou R, Benzaazoua M, Tagnit-Hamou A (2024) Assessment of hydration, strength, and microstructure of three different grades of calcined marls derived from phosphate by-products. J Build Eng 84:108640. https://doi.org/10.1016/j.jobe.2024.108640
55. Liu Y, Alessi DS, Flynn SL, Alam MS, Hao W, Gingras M, Zhao H, Konhauser KO (2018) Acid-base properties of kaolinite, montmorillonite and illite at marine ionic

strength. Chem Geol 483:191–200. https://doi.org/10.1016/j.chemgeo.2018.01.018
56. Ma H (2014) Mercury intrusion porosimetry in concrete technology: tips in measurement, pore structure parameter acquisition and application. J Porous Mater 21(2):207–215. https://doi.org/10.1007/s10934-013-9765-4
57. Zhao B, Liu L, Cheng H (2021) Rational design of kaolinite-based photocatalytic materials for environment decontamination. Appl Clay Sci 208:106098. https://doi.org/10.1016/j.clay.2021.106098
58. Wilson MJ, Wilson L, Patey I (2014) The influence of individual clay minerals on formation damage of reservoir sandstones: a critical review with some new insights. Clay Miner 49(2):147–164. https://doi.org/10.1180/claymin.2014.049.2.02
59. Koenig A (2020) Analysis of air voids in cementitious materials using micro X-ray computed tomography (µXCT). Constr Build Mater 244:118313. https://doi.org/10.1016/j.conbuildmat.2020.118313
60. Li N, Yu S, Fang J, Yu Y, Jiang P, Pu S, Wang W (2022) Performance and mechanism of illite in removing graphene oxide from aqueous solution. Appl Clay Sci 230:106711. https://doi.org/10.1016/j.clay.2022.106711
61. Zhou H (2016) Mixture of palygorskite and montmorillonite (Paly-Mont) and its adsorptive application for mycotoxins. Appl Clay Sci 131:140–143. https://doi.org/10.1016/j.clay.2016.03.012
62. Wang R, Peng Y, Zhou M, Shou D (2016) Smart montmorillonite-polypyrrole scaffolds for electro-responsive drug release. Appl Clay Sci 134:50–54. https://doi.org/10.1016/j.clay.2016.05.004
63. Florea MVA, Brouwers HJH (2012) Chloride binding related to hydration products. Cem Concr Res 42(2):282–290. https://doi.org/10.1016/j.cemconres.2011.09.016
64. Pantić V, Šupić S, Vučinić-Vasić M, Nemeš T, Malešev M, Lukić I, Radonjanin V (2023) Effects of grinding methods and water-to-binder ratio on the properties of cement mortars blended with biomass ash and ceramic powder. Mater 16(6):2443. https://doi.org/10.3390/ma16062443
65. Mboya HA, King'ondu CK, Njau KN, Mrema AL (2017) Measurement of pozzolanic activity index of scoria, pumice, and rice husk ash as potential supplementary cementitious materials for Portland cement. Adv Civ Eng 2017:1–13. https://doi.org/10.1155/2017/6952645
66. Maier M, Sposito R, Beuntner N, Thienel KC (2022) Particle characteristics of calcined clays and limestone and their impact on early hydration and sulfate demand of blended cement. Cem Concr Res 154:106736. https://doi.org/10.1016/j.cemconres.2022.106736
67. Berodier E, Scrivener K (2014) Understanding the filler effect on the nucleation and growth of C-S-H. J Am Ceram Soc 97(12):3764–3773. https://doi.org/10.1111/jace.13177
68. Antoni M, Rossen J, Martirena F, Scrivener K (2012) Cement substitution by a combination of metakaolin and limestone. Cem Concr Res 42(12):1579–1589. https://doi.org/10.1016/J.CEMCONRES.2012.09.006
69. Rodriguez C, Tobon JI (2020) Influence of calcined clay/limestone, sulfate and clinker proportions on cement performance. Constr Build Mater 251:119050. https://doi.org/10.1016/j.conbuildmat.2020.119050